Research Square

Preprints are preliminary reports that have not undergone peer review.
They should not be considered conclusive, used to inform clinical practice,
or referenced by the media as validated information.

Water Seepage Induced Deformation and Stability Control of Weakly Cemented Soft-Rock Roadway

Gangye Guo

guogangye@tdkcsj.com

CCTEG Coal Mining Research Institute

Yongzheng Wu

CCTEG Coal Mining Research Institute

Genshui Wu

Hunan University of Science and Technology

Article

Keywords: water seepage, weakly cemented soft rock, mining roadway, deformation mechanism, stability control

Posted Date: November 4th, 2026

DOI: https://doi.org/10.21203/rs.3.rs-10590736/v1

License: This work is licensed under a Creative Commons Attribution 4.0 International License.
Read Full License

Additional Declarations: No competing interests reported.

Water Seepage Induced Deformation and Stability Control of Weakly Cemented Soft-Rock Roadway

Gangye Guo [1,2,3*] Yongzheng Wu [1,2,3] Genshui Wu[4,5]

1 CCTEG Coal Mining Research Institute, Beijing 100013, China;
2 Coal Mining and Design Department,Tiandi Science & Technology Co., Ltd., Beijing 100013, China;
3. State Key Laboratory of Coal Mining and Clean Utilization,Beijing 100013, China
4. School of Resource, Environment and Safety Engineering, Hunan University of Science and Technology, Xiangtan, Hunan 411201, China
5. Sanya Institute of Hunan University of Science and Technology, Sanya 572024, China
* Correspondence: **guogangye@tdkcsj.com** (GY.G)

Abstract: Long-term groundwater seepage promotes continuous water–rock interaction, resulting in progressive deterioration of weakly cemented soft rock and posing significant challenges to the long-term stability of underground excavations. To investigate the deformation and failure mechanisms and stability control of argillaceous weakly cemented soft-rock roadways under long-term water-seepage conditions, the 110803 working face in Qingshuiying coal mine was selected as the engineering background. Field investigation, theoretical analysis, numerical simulation, and in-situ monitoring were conducted. The results indicate that the surrounding rock is dominated by argillaceous weakly cemented soft rock and has undergone significant deterioration under long-term water seepage. The original support system is characterized by a weak anchoring foundation, low prestress, and insufficient bearing capacity, which limits effective deformation control. Based on the changes in the slope and deformation rate of the convergence curve, the roadway deformation process is divided into three stages: initial rapid deformation, intermediate accelerated deformation, and late slow deformation. A coupled progressive failure mechanism involving water seepage and three weak links is identified, including water-induced softening and swelling of the roof rock, a weak anchoring foundation, a weak prestress transmission layer, and low surrounding-rock bearing capacity. These factors drive deformation from local damage toward global instability, with water–rock interaction acting as the dominant driving factor. Accordingly, a control strategy of water isolation and threefold strengthening is proposed to isolate water from the surrounding rock and enhance anchoring capacity, prestress transmission, and overall rock-mass strength. A fully enclosed support system comprising roof control, sidewall reinforcement, and floor strengthening is developed. Field application demonstrates that the proposed method effectively reduces roadway deformation and maintains long-term stability, providing a reference for the control of water-bearing soft-rock roadways.

Keywords: water seepage; weakly cemented soft rock; mining roadway; deformation mechanism; stability control

1. Introduction

Water seepage is one of the primary factors responsible for the instability of soft-rock roadways in underground coal mines. Under long-term seepage conditions, water-rock interaction alters the physical and mechanical properties of soft rock, accelerates crack propagation and structural deterioration, and significantly reduces the bearing capacity of surrounding rock. These effects become more pronounced in deep mining environments, where high in-situ stress, elevated geothermal temperature, and complex hydrogeological conditions coexist [1–3]. As a result, severe deformation and support failure frequently occur in soft-rock roadways subjected to water seepage [4–5]. According to statistics, more than 10,000 km of roadways are excavated annually in China, among which soft-rock roadways account for a

considerable proportion (>10%) [6–8]. During service, many soft-rock roadways experience roof subsidence, rib spalling, floor heave, and support failure, which not only increase roadway maintenance costs but also seriously affect the safe and efficient production of coal mines. Therefore, the stability control of soft-rock roadways has remained a critical research topic in the fields of coal mine strata control and underground engineering. Recent years have witnessed extensive studies on the deformation and failure mechanisms of soft-rock roadways and their support technologies. Significant progress has been achieved in this field. The concept of surrounding rock control has gradually shifted from passive support to active support. A collaborative support system centered on high-prestress, high-strength, and high-stiffness bolts and cables has been developed [9–11]. In addition, the development of numerical simulation, field monitoring, and geomechanical testing technologies has provided important support for stability evaluation and support parameter optimization of soft-rock roadways. To address the large deformation of deep soft-rock roadways, many researchers have investigated the failure mechanisms, support theories, and control technologies. Wang et al. [12] combined field testing, theoretical analysis, and numerical simulation to reveal the failure mechanism of an ultra-large-section soft-rock roadway at a depth of over 1000 m. They proposed and applied a collaborative control technology integrating grouting, anchoring, and shotcreting. Pei et al. [13] established an energy-driven model for analyzing large deformation in a soft-rock roadway located in the footwall of a fault. They proposed a synergistic control method combining pressure relief and reinforcement, which effectively mitigated large deformation of the surrounding rock. Liu et al. [14] investigated the asymmetric deformation characteristics and influencing factors of deep soft-rock roadways. They reduced the extent of the plastic zone and surrounding rock deformation by optimizing the support parameters.

In terms of crack evolution and instability mechanisms of surrounding rock, Ma et al. [15] investigated the crack distribution characteristics of soft-rock roadways under different lateral pressure coefficients, revealing the intrinsic relationship between crack propagation in the plastic zone and large deformation of surrounding rock. Sun et al. [16] evaluated the risk of squeezing-induced large deformation in deep soft-rock roadways based on hydraulic fracturing in-situ stress measurements, and identified high horizontal tectonic stress as a key factor inducing surrounding rock instability. Yan et al. [17] studied the creep damage mechanism of deep soft-rock roadways through triaxial creep tests and numerical simulations, concluding that high stress concentration and rock mass fragmentation jointly contribute to the progressive development of long-term deformation. Considerable attention has also been paid to the stability control of water-rich soft-rock roadways. Lin et al. [18] investigated deformation characteristics and support optimization methods for such roadways, proposing a gradient support technology that effectively controls floor heave and rib deformation. Lu et al. [19] proposed a self-dissolving grouting reinforcement method that utilizes groundwater within the surrounding rock to enhance slurry diffusion and improve reinforcement performance in water-rich soft rock. Zhang et al. [20] developed a cable–truss coupled support system and demonstrated its effectiveness in restraining plastic zone expansion under fluid–solid coupling conditions. He et al. [21] focused on floor heave in water-rich soft-rock roadways and revealed that hydraulic action combined with mining-induced stress leads to floor instability, further proposing a “double-sealing + inverted arch” control technology. Wang et al. [22] analyzed roof instability mechanisms in water-rich environments and identified strength degradation induced by water–rock interaction as a primary cause of failure, while showing that optimization of roadway geometry and support parameters significantly improves stability. Fan et al. [23] examined long-term groundwater effects on coal roadway instability and proposed a collaborative control strategy combining grouting and high-strength support, achieving long-term stability of the surrounding rock.

Most existing studies have focused on general soft-rock roadways. However, for mining roadways affected by long-term water seepage, a systematic understanding of the strength deterioration law, stress redistribution characteristics, and deformation and failure evolution mechanism of the surrounding rock is still lacking. In particular, under the coupled effects of mining disturbance and water softening, the surrounding rock structure continuously weakens, and the bearing capacity of support components gradually decreases. This leads to nonlinear large deformation and repeated instability of the roadway, which brings great difficulty to long-term stability control [24–25]. Water seepage not only changes the physical and mechanical properties of soft rock, but also accelerates crack propagation and the degradation of structural

planes, thereby reducing the overall bearing capacity of the surrounding rock. For mining roadways, the combined effects of mining-induced stress concentration, surrounding rock damage, and water–rock interaction make the deformation and failure mechanism more complex [26]. Therefore, revealing the deformation and failure mechanism of water-seepage soft-rock mining roadways and identifying the key controlling factors are of great theoretical significance. It is also of important engineering value to establish a targeted support and control system for safe and efficient deep mining. [27–30].

To address these problems, the water-seepage affected soft-rock mining roadway in Qingshuinying Coal Mine was studied using field investigation, geomechanical testing, ground pressure monitoring, numerical simulation, and engineering practice. The deformation and failure characteristics and their evolution laws were systematically analyzed. The instability mechanism under coupled mining disturbance and water-induced softening was revealed, and the key controlling factors of large deformation were identified.The surrounding rock exhibits the typical “one water and three weaknesses” characteristics, including water-bearing strata, weak anchoring, weak prestress transmission, and low bearing capacity. Water is identified as the dominant factor inducing severe deformation. A control concept of “one isolation and three strengthening” was proposed for weakly cemented soft rock roadways. Based on this, a fully enclosed support system of “roof control, sidewall reinforcement, and floor strengthening” was developed. The results provide a reference for stability control of similar roadways and support safe deep coal mining.

2 Engineering overview

2.1 Roadway layout

Qingshuiying coal mine is located in the Ningxia Hui Autonomous Region. The primary coal seams currently being mined are Nos. 2 and 8. The surrounding rock along these seam extraction routes is characterized as argillaceous soft rock. The roof of the No. 2 coal seam extraction route consists of argillaceous, poorly cemented sandstone, which is soft and easily eroded. The floor is composed of argillaceous sandstone, mainly consisting of highly expansive illite and chlorite, making it prone to swelling upon water exposure. The surrounding rock exhibits poor engineering geological properties, classifying it as a typical soft-rock roadway. These roadways deform significantly during both driving and extraction, causing roof subsidence and localized fracturing. This leads to failure of the anchor support system, with individual bolts being pulled out or broken. These issues are typically accompanied by water seepage and dripping.

The 110803 operational face of the Qingshuiying coal mine is situated in the north wing of the No. 11 mining area. The vertical depth from the working face to the surface ranges from 197.73 m to 325.5 m, with a mean of 261.6 meters. The strike length of the working face is 2,998 meters, while the dip length is 260 meters. It is bounded to the east by solid coal from the No. 8 seam, to the south by the 1172 horizontal reverse crosscut connecting roadway, to the west by a 63-243 m protective coal pillar left by the No. 8 coal wind oxidation zone, and to the north by the boundary protective coal pillar of the No. 11 mining area. As demonstrated in Fig. 1, there is currently no other mining or driving activity in the area. The 110803 transport roadway is intended to be 3,018 metres long; 735 metres have already been excavated, leaving 2283 metres to drive. The principal ceiling of the 110803 working face is a cracked and porous confined aquifer of coarse-grained sandstone from the fifth member of the Yan'an Formation. The thickness varies from 0.80 m and 29.56 m, with an average of 6.52 m. This aquifer, located 0.45–15.03 meters from the No. 8 coal seam, has limited water flow and poor permeability. However, during the driving process, water from this sandstone aquifer seeps onto the working face via water-conducting channels such as sandstone pores, fissures, and anchor cable holes in the highway roof, serving as the primary source of water for the working surface. Water from this aquifer will cause leaking on certain sections of the roadway. When exposed to water, the roadway floor argillizes and softens, which can quickly degrade manufacturing conditions. The No. 8 coal seam has a natural density of 1.96 g/cm3, with an uniaxial compressive strength of 11 MPa, an elastic modulus of 4.8 GPa, a Poisson's ratio of 0.25, a cohesion of 1.1 MPa and an internal friction angle of

20°, indicating a low-strength, weakly cemented coal seam that is significantly weaker than the surrounding siltstone and sandstone strata.

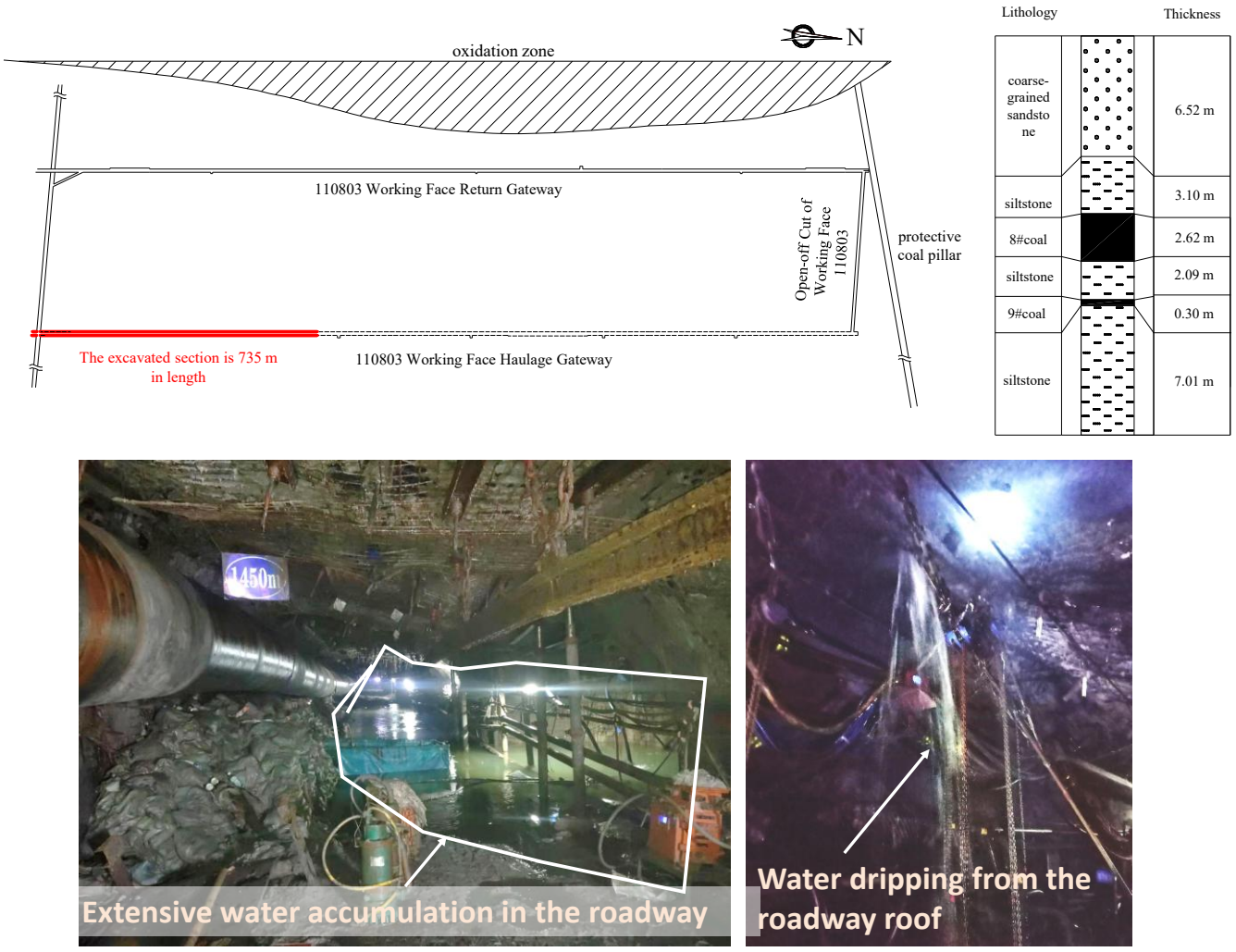


Fig.1 Schematic diagram of the transportation roadway

2.2 Roof and floor lithology of soft rock roadways

The immediate floor is siltstone, the main floor is a combination of the No. 9 coal seam and siltstone, and the roofs are siltstone and coarse sandstone, respectively. The main roof's coarse sandstone ranges in thickness from 8.74 m to 11.08 m, with an average of 9.91 m. It is grey, contains a small quantity of coal particles and plant fossils, and has horizontal bedding. The immediate roof's siltstone ranges in thickness from 1.92 m to 2.80 m, with an average of 2.36 m; it is grey, soft, predominantly quartz with a trace of mica, has argillaceous cementation, and is interspersed with thin layers of mudstone and coal streaks. The No. 8 coal seam varies in thickness from 1.42 m to 3.81 m, with an average of 2.62 m. It is black with a pitch-like sheen, classified as semi-dull coal, composed mostly of dull coal, and interspersed with vitrain bands. The adjacent floor's siltstone thickness varies from 1.30 m to 3.57 m, with an average of 2.09 m. It is grayish-black, relatively firm, and compact, with argillaceous cementation, thin layers of mudstone, and coal streaks that melt when exposed to water. The main floor's No. 9 coal streak ranges in thickness from 0.14 m to 0.72 m, with an average of 0.30 m. It is black, interspersed with vitrain bands and fusain, and classified as semi-dull coal. The main floor's siltstone ranges in thickness from 0.86 m to 17.64 m, with an average of 7.01 m; it is grey, relatively hard, has horizontal bedding, contains plant fossils, has argillaceous cementation, is interspersed with thin coal streaks, has an uneven fracture, and is relatively soft and friable.

2.3 Damage conditions of soft rock roadways

As shown in Fig. 2, the 110803 transportation roadway features a round arch cross-section. The roadway's clear width is 5400 mm, height is 3600 mm, and cross-sectional area is 14.64 square meters. The original support rock bolts are Φ22×2500 mm left-hand threaded steel bolts without longitudinal ribs, with a spacing and row pitch of 1000 × 1000 mm. To anchor resin cartridges, at least 200 N·m of pre-tightening torque and 190 kN of anchoring force are required. The matching bearing plates are butterfly-shaped Q235 steel plates measuring 150×150×10 mm in size. Cable bolts (Φ21.8×5300 mm) are utilised, with a spacing and row pitch of 1500×1000 mm. Their pre-tightening force is no less than 150 kN, while their anchoring force is no less than 350 kN. The matching bearing plates measure 300 × 300 × 16 mm. Steel reinforcement mesh is comprised of Φ6.5 mm round steel with a mesh size of 100 × 100 mm. Another mesh is built from Φ16 mm circular steel and measures 50×70 mm.

The anchor cable supporting beams are constructed from No. 11 mining I-beams (26.05 kg/m) with the following dimensions: height h is 110 mm, leg width b is 90 mm, web thickness d is 9 mm, and length L is 2000 mm. The external bearing plates are steel plates measuring 150 × 150 × 10 mm. The floor paving concrete and shotcrete have strength grades of C30.

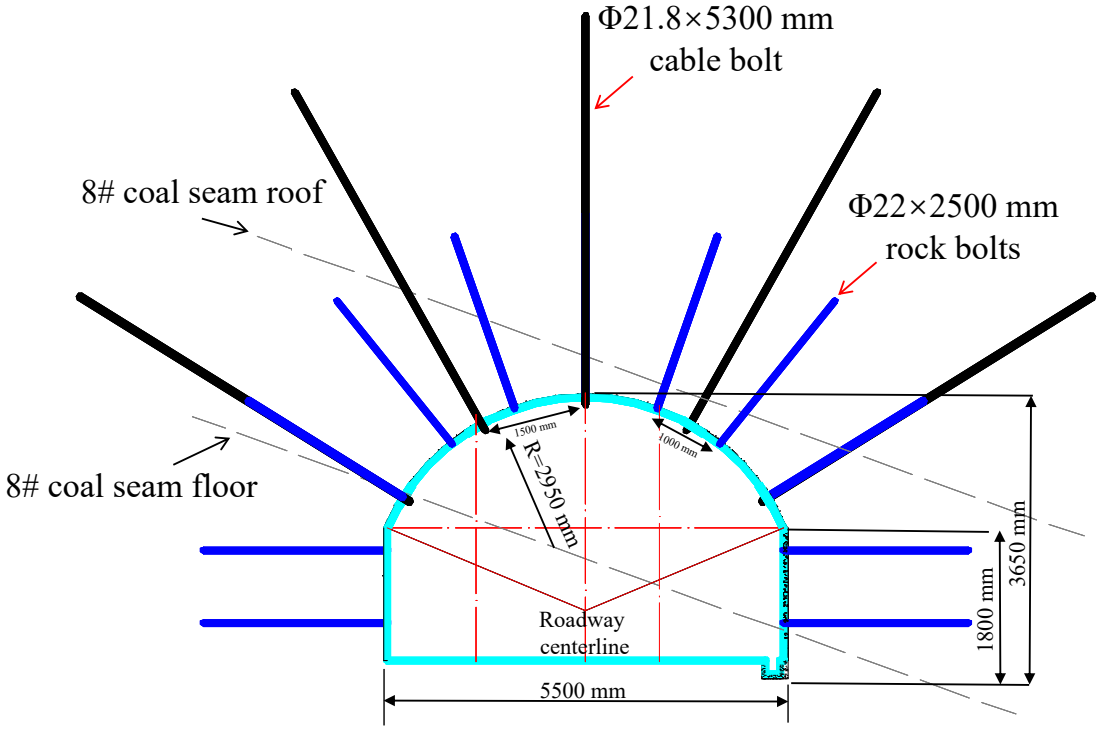


Fig.2 Original support scheme for the 110803 transportation roadway

Currently, the 110803 transportation roadway is experiencing varying levels of rock pressure manifestations. The degree of deformation and failure of the roadway floor varies significantly, and highly distorted areas have already hampered the roadway's routine operations. Deformation and failure situations are found in a variety of regions, including normal parts, dripping sections, and showering sections; Fig. 3 depicts photographs of the roadway's overall condition. The 110803 transportation roadway exhibits varying degrees of deformation and failure. Roof subsidence and cracking are obvious, and mesh bagging is extremely prevalent. The ribs are converging inward, and the floor strata are argillized, softened, and swelled, causing floor heave. According to on-site examinations, in areas with considerable floor deformation, the floor heave exceeds 700 mm, the roof sinking is around 300 mm, and the inward convergence of the two ribs is greater than 600 mm. The roof mesh has ripped in places, and the anchor wires are heavily corroded. Furthermore, the surface-retaining components in the support design work poorly. The I-beams only make linear contact with the roof's surrounding rock, failing to evenly distribute the pre-tightening force over the deeper rock mass. While the support system is currently under moderate stress and has not undergone large-scale deformation or failure, the

roadway's underlying rock remains damp due to water seepage and rain. The residual water from showering is apparent locally on the floor surface.



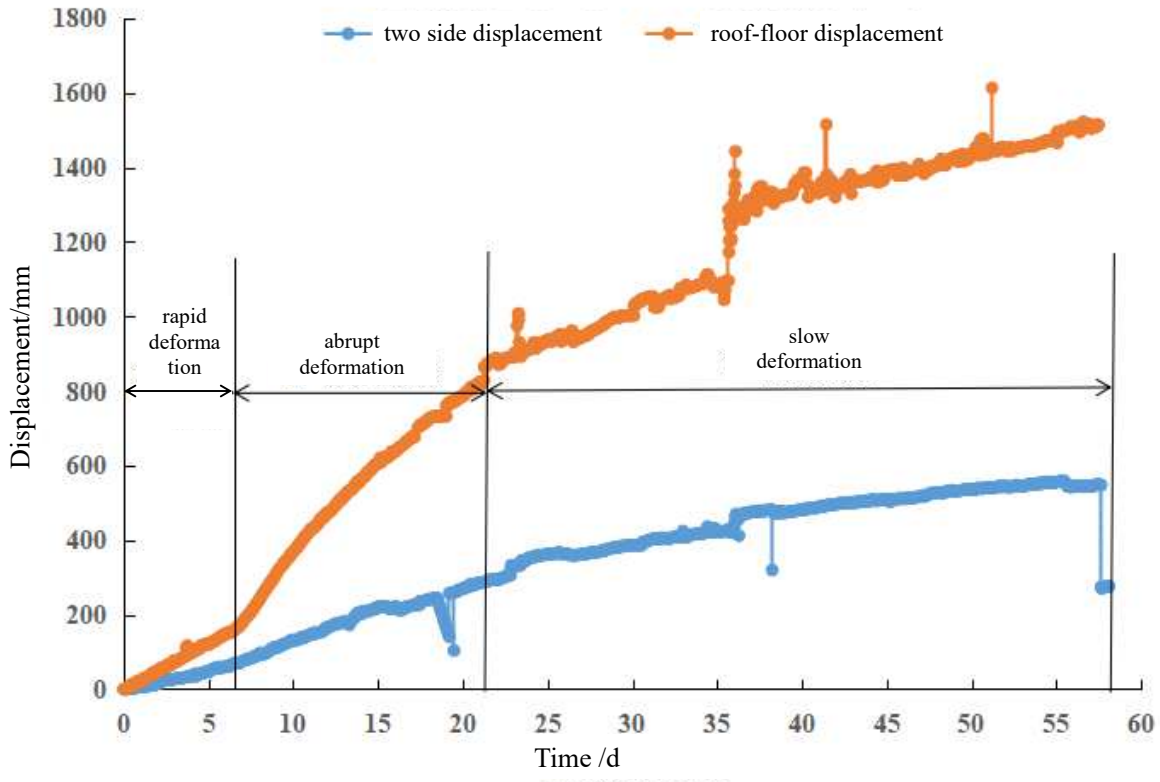
Fig.3 Field photos showing deformation and damage in the 110803 transportation roadway

The 110207 transportation roadway is located near the 110803 transportation roadway and has similar geological conditions. Since its excavation, severe deformation and localized collapse have occurred, mainly due to roof dripping water and weak surrounding rock. Fig. 4 shows the deformation curve and real-time laser-based displacement monitoring system for surrounding rock in roadways. It is obvious that the deformation and failure of this type of pavement exhibit the following features:

(1) The surrounding rock has deformed significantly, resulting in severe floor heave. During the driving phase, rock pressure manifestations are severe, including roof sinking, inward convergence of the two ribs, and substantial floor heave. During nearly 60 days of observation, the roof-to-floor convergence surpassed 1,400 mm, and the rib-to-rib convergence exceeded 400 mm, while the adjacent rock deformation increased. Over 30% of the excavated roadway, which is almost 2,300 meters long, is severely twisted and damaged.

(2) Prolonged and staged deformation. The surrounding rock continued to deform throughout the monitoring period. As shown in Fig. 4, the deformation process can be divided into three stages according to the changes in the slope and deformation rate of the convergence curve: an initial rapid-deformation stage (0–7 d), an intermediate accelerated-deformation stage (7–21 d), and a late slow-deformation stage (after 21 d). During the initial stage, the roof-to-floor convergence increased rapidly and exceeded 200 mm within approximately 7 d. During the intermediate stage, the convergence increased by more than 600 mm within 14 d, indicating a pronounced acceleration in deformation. In the late stage, the deformation rate gradually decreased, although the surrounding rock continued to deform for more than 30 d. This persistent deformation indicates that the roadway surrounding rock remained in an unstable deformation state for a prolonged period.

(3) Significant deformation of the surrounding rock. The deformation was particularly pronounced in the roof-to-floor direction. During the approximately 60-day monitoring period, the roof-to-floor convergence exceeded 1,400 mm, while the rib-to-rib convergence exceeded 400 mm. The large cumulative deformation and prolonged deformation period indicate a strong tendency for continuous deformation of the surrounding rock. Such pronounced deformation substantially increases the difficulty of maintaining the stability of the soft-rock roadway in Qingshuiying coal mine.



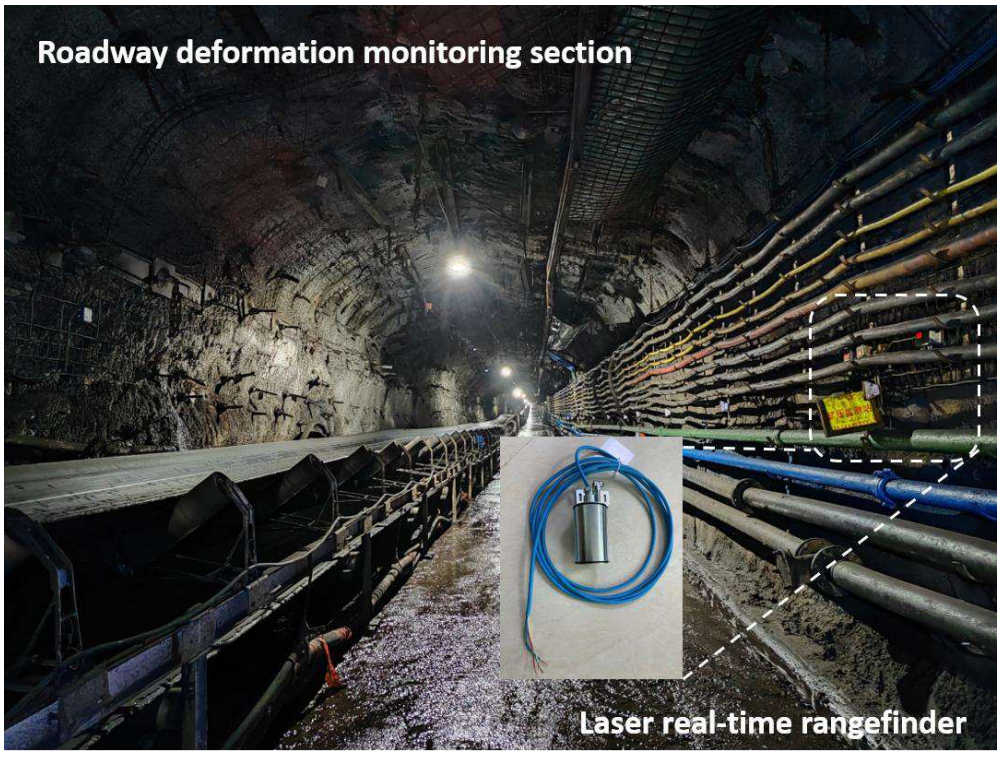


Fig.4 Deformation curve and real-time laser-based displacement monitoring system for surrounding rock in roadways

3 Geomechanical characteristics of soft rock roadways

3.1 Fracture characteristics

Fig. 5 depicts the borescope inspection results of the roof structure at 150 meters, which clearly indicate internal structures, striations, and pores. A 0-1.4 m fracture growth zone can be found 150 m up on the top of the 110803

transportation roadway. This length, which ranges from 0.7 m to 0.9 m, comprises numerous longitudinal and transverse fractures with poor integrity and significant instability, indicating that it is a zone of very dense fracture formation. At 4.3–4.7 m, multiple transverse coal streaks can be visible, indicating somewhat extensive fracture development. Transverse fractures are occasionally seen between 5.0 and 8.0 m; these fractures are only slightly developed, indicating adequate rock integrity. From 9.0 to 10.2 m, there are clear shallow drill damage zones, as well as severe argillization and water-showering zones, indicating that the rock stratum is intact but compromised.

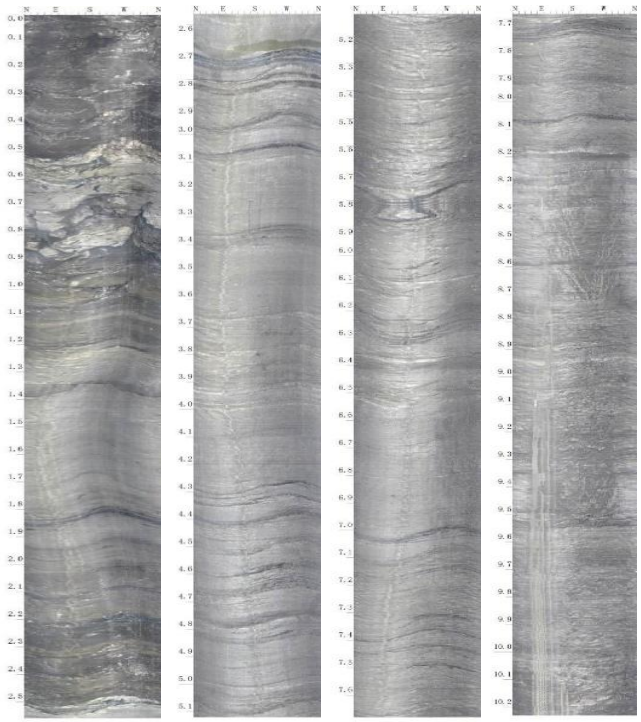


Fig.5 Borescope image of the roadway roof at 150 m

As shown in Fig. 6, due to substantial internal collapse and blockage within the borehole, the borescope investigation of the rib structure at 150 m could only reach a depth of around 7.4 m. The inspection results are clear, showing internal structures, striations, pores, and other features. Fracture development zones are located 50 meters into the rib of the 110803 transportation roadway. Many sets of transverse fractures are observed between 0.0 m and 0.7 m, indicating a zone of very dense fracture development, with the remainder being minimally developed fracture zones. From 3.5 m to 7.4 m, there is visible fracture growth and hollow zones, indicating that the rock layers are not structurally stable.

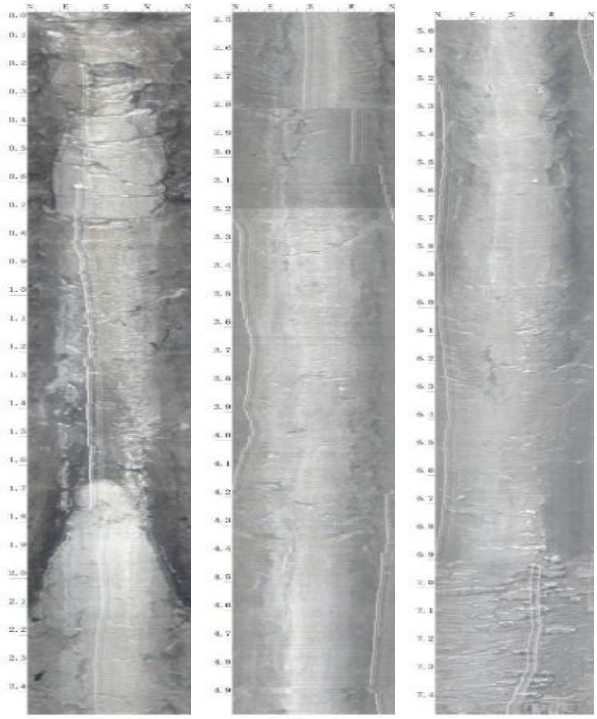


Fig.6 Borescope image of the roadway rib at 150 m

3.2 Mineral composition

As shown in Tables 1 and 2, the clay mineral content of roof rock at the driving face of the 110803 return airway reaches 40.2%, 41.2% and 37.8%, falling within a high proportion range. Among clay minerals, smectite accounts for 23%, 37% and 28%; illite accounts for 10%, 8% and 11%; kaolinite accounts for 55%, 46% and 50%; chlorite accounts for 12%, 9% and 11%. From lithology classification, this stratum exhibits prominent water-softening and disintegration characteristics. All types of clay minerals absorb water and expand, differing only in the magnitude of hydration swelling. Higher clay mineral content leads to more significant hydration and swelling effects.

Hydration swelling is controlled by three forces: surface hydration force, osmotic hydration force and capillary force. Montmorillonite, illite and kaolinite are all aluminosilicates with lamellar crystal structures. Under anhydrous conditions, the interlayer spacing is extremely small; when exposed to water, a large volume of water is adsorbed and filled between layers. Further reactions of clay molecules induce hydrolysis into H^+ cations and OH^- anions, forming hydrated clay with distinct colloidal properties, including expansibility, rheology, dispersibility and flocculation. Macroscopically, this phenomenon manifests in the 110803 return airway as mudstone swelling, fragmentation, dispersive disintegration, or flocculent fluidization accompanied by sharp strength degradation, which severely threatens the stability of roadway surrounding rock. In summary, roadways in Qingshuinying coal mine are typical large-deformation roadways excavated in argillaceous weakly cemented soft rock under weak aquifer conditions. The X-ray diffraction patterns of non-clay minerals and clay minerals of rock samples are attached as direct evidence for the table data, as shown in Fig. 7.

Table 1 Mineral X-ray diffraction analysis

Sample No.	Mineral content (%)					
	Quartz	K-feldspar	Plagioclase	Siderite	Pyrite	Clay minerals
1-1	40.0	5.9	8.9	1.8	3.2	40.2
1-2	45.5	4.0	6.6	2.0	0.7	41.2
1-3	35.5	20.0	4.4	2.3	/	37.8

Table 2 Clay mineral X-ray diffraction analysis report

Sample No.	Relative content of clay minerals (%)						Mixed-layer ratio (%S)	
	S	I/S	It	Kao	C	C/S	I/S	C/S
34	23	/	10	55	12	/	/	/
35	37	/	8	46	9	/	/	/
36	28	/	11	50	11	/	/	/

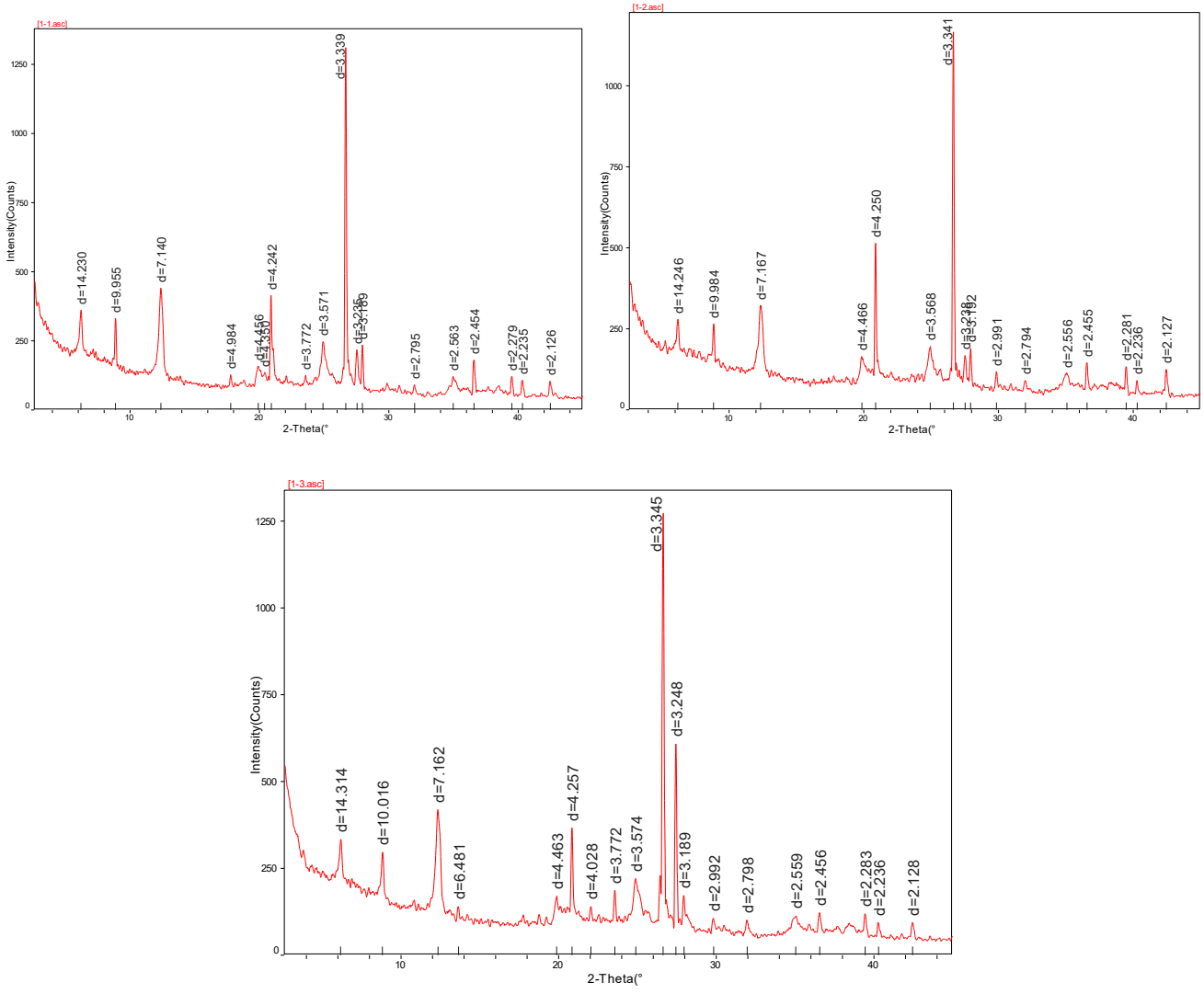


Fig. 7 X-ray diffraction pattern of non-clay minerals in the rock sample of the bottom plate of the mining roadway in working face 110803

3.3 Mechanical properties

In accordance with laboratory rock sampling standards, rock cores with a depth of 8 m were collected from the mining roadways of 110207 and 110803 working faces for laboratory testing. Test items include uniaxial compressive strength, uniaxial tensile strength, elastic modulus and Poisson's ratio. The rock sample processing and testing procedures are shown in Fig. 8.



Fig. 8 On-site photographs of sample collection, processing, and testing

Due to the weak and highly moisture-sensitive nature of the surrounding rock, most specimens collected from the 110803 working face were in a natural-moisture condition, while representative dry and saturated specimens were difficult to obtain; therefore, the available dry- and natural-moisture-state mechanical parameters are presented in Table 3 for comparison. As listed in Table 3, the mechanical properties of surrounding rock vary significantly in different zones of the 110803 working face, presenting obvious heterogeneous characteristics. Within the 1–8 m range of the transportation roadway roof, the uniaxial tensile strength of rock strata is merely 0.19–0.27 MPa, the uniaxial compressive strength ranges from 2.72 to 3.08 MPa, and the elastic modulus is lower than 0.40 GPa. These strata belong to typical weak fractured rock masses with poor resistance to tensile failure and compressive deformation, prone to crack propagation and large deformation instability under mining disturbance.

In contrast, the mechanical performance of rock strata within 1–4 m of the return airway roof is greatly improved, with an average uniaxial tensile strength of 3.00 MPa, an average uniaxial compressive strength of 38.11 MPa and elastic modulus up to 11.14 GPa. This zone contains intact hard rock strata with strong bearing capacity and overall stability. Nevertheless, the rock strength decreases again in the 5–8 m range of the return airway roof, with tensile strength of only 0.244 MPa and compressive strength reduced to 5.25 MPa, indicating weak interlayers or weathered fractured zones above the hard rock stratum, which easily form weak interlayer planes. The mechanical properties of rock strata within 1–4 m of the return airway floor fall between the above two cases, possessing moderate bearing capacity but still classified as medium-low strength rock masses as a whole. Comprehensive analysis demonstrates that the surrounding rock of the 110803 working face presents an alternating "soft-hard-soft" distribution pattern. The roof of the transportation roadway and deep roof strata generally have low strength, serving as weak zones for roadway

stability control; while the shallow roof of the return airway forms a relatively stable key bearing stratum. Such remarkably heterogeneous mechanical structures lead to non-uniform surrounding rock deformation and stress distribution, which constitute critical inducements for roof separation, crack propagation and local instability. Therefore, differentiated zonal and layered support strategies should be adopted in roadway support design considering discrepancies in mechanical parameters of rock strata at different depths, to improve the overall bearing capacity and long-term stability of surrounding rock.

Table 3 Statistical mechanical parameters of surrounding rock in the 110803 working face

Location	Depth range /m	Average uniaxial tensile strength /MPa	Average uniaxial compressive strength/MPa	Average elastic modulus/GPa	Average Poisson's ratio
Transportation roadway roof (Naturally hydrated)）	1～3	0.27	3.08	0.39	0.33
Transportation roadway roof (Naturally hydrated)	4～8	0.19	2.72	0.278	0.363
Return airway roof (dry)	1～4	3	38.11	11.14	0.13
Return airway roof (Naturally hydrated)	5～8	0.244	5.25	0.67	0.34

4 Deformation and failure mechanism of water-rich soft rock roadways

4.1 Numerical analysis

To clarify the deformation and failure characteristics of the 110803 transportation roadway under the original support scheme and reveal the corresponding failure mechanism of the soft rock roadway surrounding rock, a numerical calculation model was established based on the original support design and geological data of the 110803 transportation roadway. The model dimension is 75 m × 75 m × 10 m; the upper boundary is free, and the lower boundary is fully fixed. Uniform vertical stress of 4.6 MPa is applied on the upper boundary. The numerical model of the roadway is shown in Fig. 9(a). Combined with field measurements and geomechanical parameters of adjacent coal mines, the maximum horizontal in-situ stress σ_H = 8.07 MPa, vertical in-situ stress σ_v = 4.60 MPa, and lateral pressure coefficient λ = 1.75. With reference to the national standard GB50218-94 for engineering rock mass classification, physical and mechanical parameters for numerical simulation were back-calculated and listed in Table 4 based on field conditions.

Table 4 Stratum mechanical parameters for numerical simulation

No.	Internal friction angle φ/°	Cohesion c/MPa	Compressive strength/MPa	Elastic modulus E/GPa	Density g/cm^3	Poisson's ratio	Tensile strength /MPa	Dilation angle /°
Siltstone	26	1.7	24	10.5	2.49	0.13	2.5	8
Coarse-grained sandstone	30	1.2	22	12.6	2.05	0.22	1.8	10
Mudstone	20	0.6	14	3.7	2.03	0.33	0.27	3
No.8 Coal	20	1.1	11	4.8	1.96	0.25	0.20	2

seam								
Floor coal streak	21	0.8	16	2.6	2.02	0.36	0.33	2

It should be noted that the numerical model in this study is a static, purely mechanical model. The seepage field, pore-water pressure, and hydro-mechanical coupling are not explicitly simulated; instead, the weakening effect of long-term water seepage is reflected by assigning the water-affected strata the reduced mechanical parameters obtained from the laboratory water-induced degradation tests (Table 3). Accordingly, the water-induced deterioration mechanism is interpreted from the integrated field observations and laboratory results, while the numerical simulation focuses on the static mechanical response of the surrounding rock under the original support scheme with these degraded parameters.

The numerical model was built using FLAC^{3D} (version 6.0, Itasca Consulting Group). An elastic – plastic constitutive model with the Mohr – Coulomb yield criterion was adopted for the rock mass. The model is discretized into hexahedral elements with a size of approximately 0.5 - 1.0 m around the roadway and 2 - 3 m in the far field. The mesh of the roadway key area was refined to a size of approximately 0.5 m, and that of the far-field rock mass was 2.0 m, consistent with the mesh schemes adopted in previous FLAC^{3D} simulations of similar weakly cemented soft-rock roadways[31]. The roadway was excavated in one stage, and the support structures were installed immediately after excavation. Rock bolts and cable bolts were modeled using built-in cable structural elements, the bearing plates using shell elements, and the shotcrete layer using solid elements. The grout annulus between the reinforcement and the borehole wall was described by the bond – slip model of the cable element. The main parameters of the support elements are listed in Table 5.

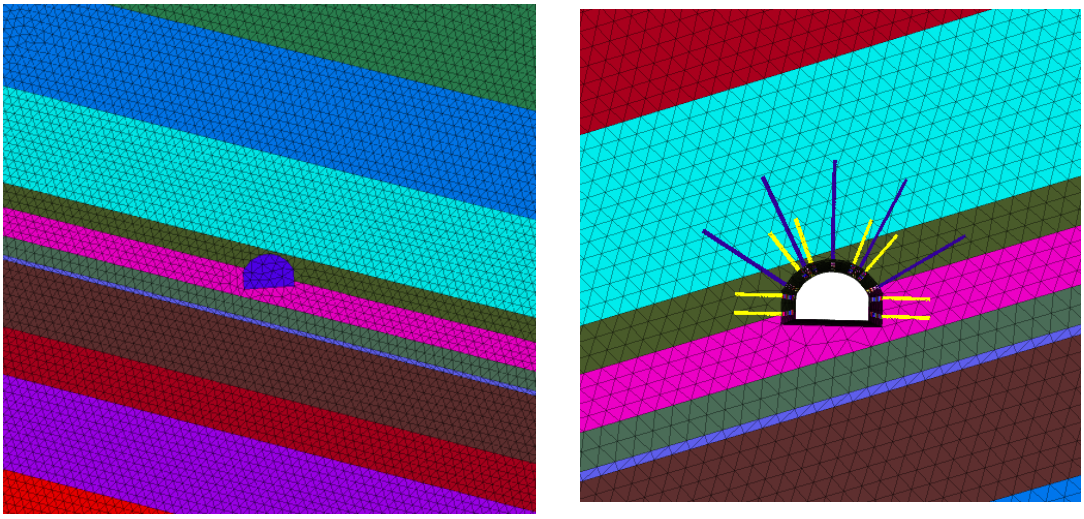
Table 5 Parameters of support elements in the numerical model

Support element	Element type	Elastic modulus /GPa	Poisson's ratio	Pretension /kN	Tensile strength /MPa	Grout cohesion /MPa	Grout friction angle /°	Grout stiffness /GPa
Rock bolt	Cable element	210	--	20	360	5.0	33	1000
Cable bolt	Cable element	210	--	70	360	5.0	33	1000
Bearing plate	Shell element	210	0.30	--	--	--	--	--
Metal mesh + shotcrete	Shell element	28	0.25	--	--	--	--	--

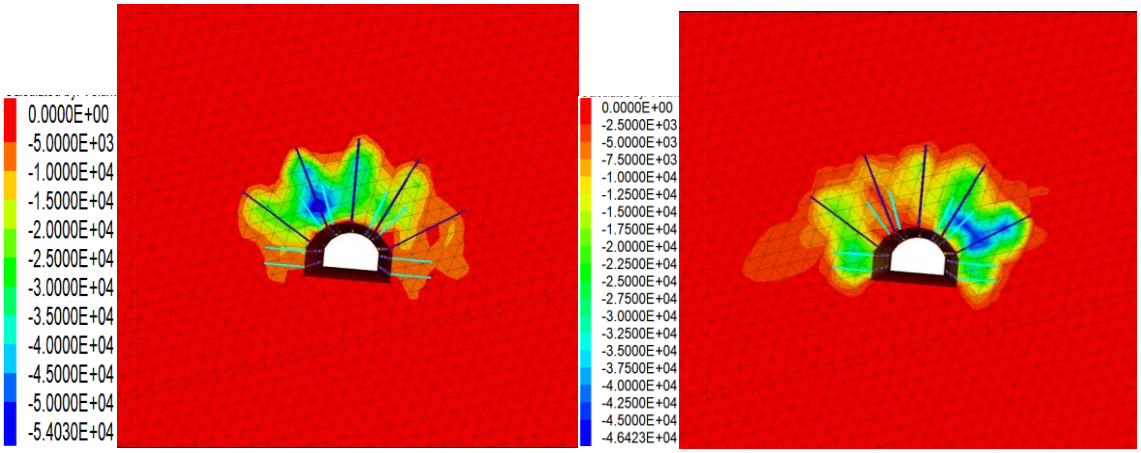
As shown in Fig. 9(b), the pre-tightening force of rock bolts under the original support scheme is only 20 kN. Under this condition, sidewall bolts fail to form continuous vertical compressive stress zones in the horizontal direction of both ribs, and no obvious compressive stress concentration appears near the right arch crown; these regions are weak support zones in the horizontal direction. Cable bolts can only form interlaced compressive stress zones above the left arch crown, with a maximum stress value of merely 0.04 MPa. The compressive stress zones generated by rock bolts at the arch crown are narrow and disconnected, leading to poor control of the roof.

Fig. 9 (c) illustrates that the vertical support stress field formed by rock bolts at the arch crown is extremely limited and distributed discretely, with a negligible squeezing control stress of only 0.02 MPa on surrounding rock. With a pre-

tightening force of 70 kN, cable bolts can form a compressive stress zone with a width of approximately 1.0 m within the cable anchorage range, and the average stress inside the zone is around 0.046 MPa. It can be concluded that both the range and magnitude of support stress fields induced by rock bolts and cables under the original support scheme are insufficient to restrain large deformation of soft rock, inevitably resulting in surrounding rock deformation and failure in the later stage.



(a) Roadway model and simulated support scheme

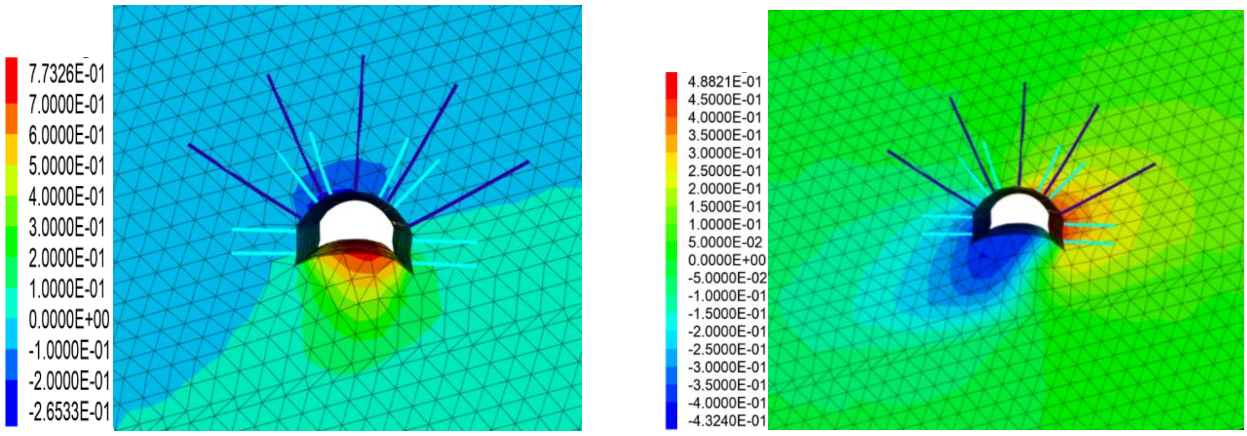


(b)Horizontal support stress field (c)Vertical support stress field

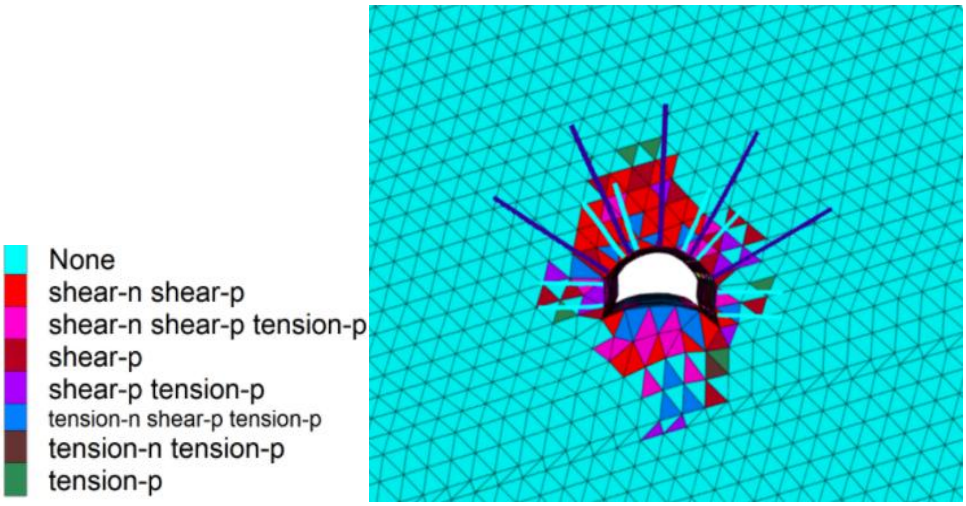
Fig.9 Numerical calculation model of the roadway

An explicit iterative solution was performed for the model, and the simulated deformation and failure morphology of the roadway surrounding rock are presented in Fig.10. Comparative analysis of Fig. 10 (a) and Fig. 10(b) reveals severe deformation and failure of the 110803 transportation roadway under the original support scheme, with overall section shrinkage exceeding 40%. Rock strata within 5.0 m depth of the floor experience varying degrees of damage, and the failure depth of surrounding rock on both sidewalls reaches 2.0 m. Displacement cloud contours indicate that the most intensive deformation occurs at the floor with floor heave over 0.8 m; the maximum roof subsidence at the central crown exceeds 0.26 m, the inward convergence of the left rib exceeds 0.35 m, and the inward convergence of the right rib exceeds 0.45 m.

Fig. 10 (c) shows that the plastic zone of surrounding rock in the 110803 transportation roadway has a wide range and irregular shape, corresponding to differential deformation and failure in various roadway parts. The maximum plastic zone boundary extends 5.3 m into the floor, 2.5 m into the left rib, 2.0 m into the right rib and 4.0 m into the roof. Shear and tensile failure coexist in the floor and sidewalls, while shear failure dominates the roof, demonstrating the low bearing capacity of surrounding rock masses.



(a) Vertical displacement (b) Horizontal displacement



(b) Plastic zone distribution

Fig.10 Deformation and failure morphology of roadway surrounding rock

4.2 Mechanism analysis

(1) Inducements of **Deformation and Failure**

Combined with field investigation, in-situ measurement and deformation-failure characteristics of roadway surrounding rock, primary factors triggering deformation and failure of soft rock roadways under weak aquifer conditions are summarized as follows:

Low strength and weak bearing capacity of surrounding rock. The average rock strength of the roof in the 110207 transportation roadway is 15 MPa, and the average strength of coal-rock mass on sidewalls is 11 MPa. Structural fractures are well-developed within 5.5 m of the roof surrounding rock. Such rock masses possess low intrinsic strength and poor integrity without sufficient bearing capacity.

High content of clay minerals and roof water seepage. X-ray diffraction tests verify that clay mineral content in surrounding rock exceeds 30%, including expansive minerals such as kaolinite and montmorillonite. These high-proportion clay minerals easily swell and disintegrate once exposed to roof dripping water.

Weak anchoring foundation of rock bolts and cables, resulting in unstable bonding between anchor components and surrounding rock. Fractures are widely developed in roadway surrounding rock, leading to poor borehole wall integrity and loose bonding between anchoring agent and rock mass. Coupled with water-rock interaction in mudstone, the shear bonding strength between anchoring agent and borehole wall is drastically reduced. Field pull-out tests show that the anchoring force of more than 30% of bolts and cables in water seepage zones is less than 80 kN.

Unreasonable design of the original support scheme incompatible with large deformation of soft rock roadways. The original support system fails to achieve full coupling with surrounding rock, equipped with small-area and low-

strength surface protection components, leading to limited overall control capacity for roadway surrounding rock. Field measurement indicates that the pre-tightening force applied on partial rock bolts and cables is merely 20 kN and 70 kN respectively, unable to realize active support effect. In particular, the neglect of floor support easily induces severe floor heave.

(2) Mechanism of deformation **and failure in roadways**

To intuitively analyze the deformation and failure evolution process of soft rock roadway surrounding rock, superficial surrounding rock deformation data were sorted into deformation curves, as shown in **Fig.11.**

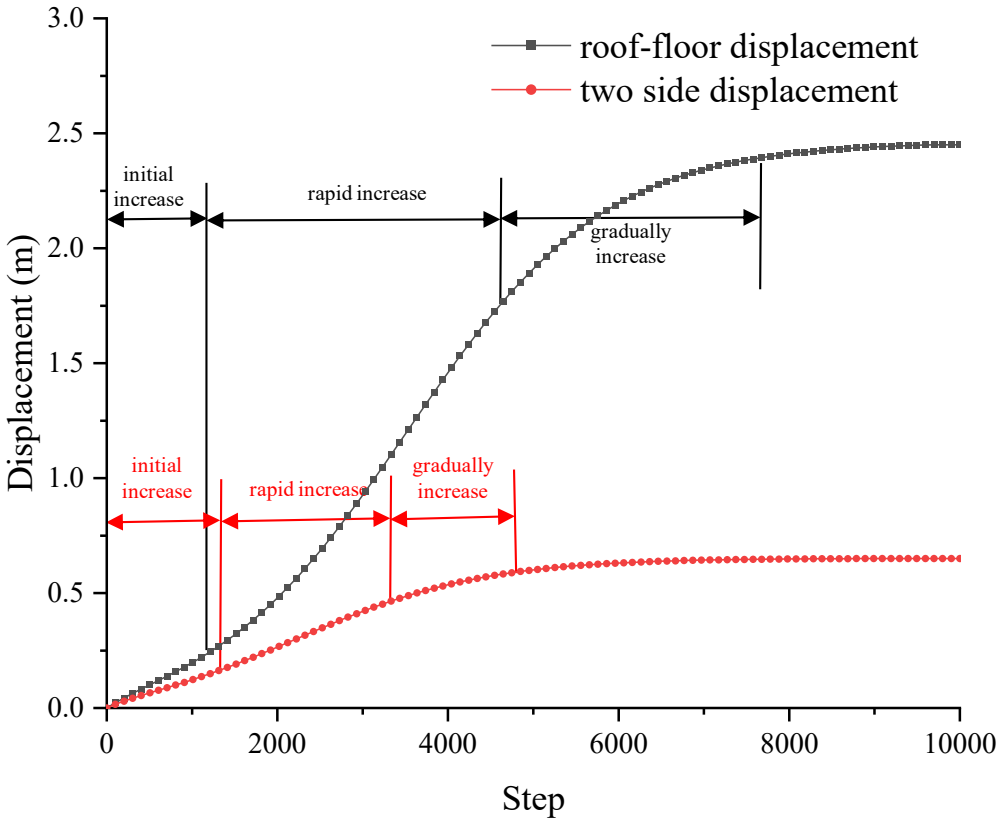


Fig.11 Simulated deformation curve of roadway surrounding rock

Fig.11 indicates that the deformation characteristics of roadway surrounding rock are consistent with the field-measured curves in **Fig.4,** and the whole deformation-failure process can be divided into three stages: initial rapid growth, medium-rate growth and slow growth. A conceptual model was established to elaborate the deformation and failure mechanism, as shown in **Fig.12.** Analysis of **Fig.12** shows that after excavation of soft rock roadway a under weak aquifer conditions, the original stress equilibrium σ of surrounding rock is broken and secondary stress redistribution occurs. If low pre-tightening force *P* of rock bolts cannot actively restrain superficial rock deformation in a timely manner, deformation and failure inevitably emerge in shallow low-strength surrounding rock.

With continuous deformation of roadway surrounding rock, fractures gradually propagate, and joints, fissures and anchor cable boreholes interpenetrate to form complex water-conducting networks connected with weak aquifers. Water reacts with high-content clay minerals in surrounding rock, not only triggering rock swelling and disintegration, but also weakening the shear bonding strength τ between anchoring agent and borehole wall. As stress balance transfers toward deep rock mass, roadway surrounding rock deformation enters the rapid growth stage. After intense deformation of shallow surrounding rock releases partial rock stress, the deformation rate slows down and stress transfers deeper into

rock mass, entering the slow growth stage. During this stage, continuous fracture propagation, water-clay mineral reaction or other factors cause debonding among anchoring agent, anchor rod/cable and borehole wall, leading to failure of bolt-cable support and subsequent severe mine pressure manifestations such as large surrounding rock deformation or roof collapse.

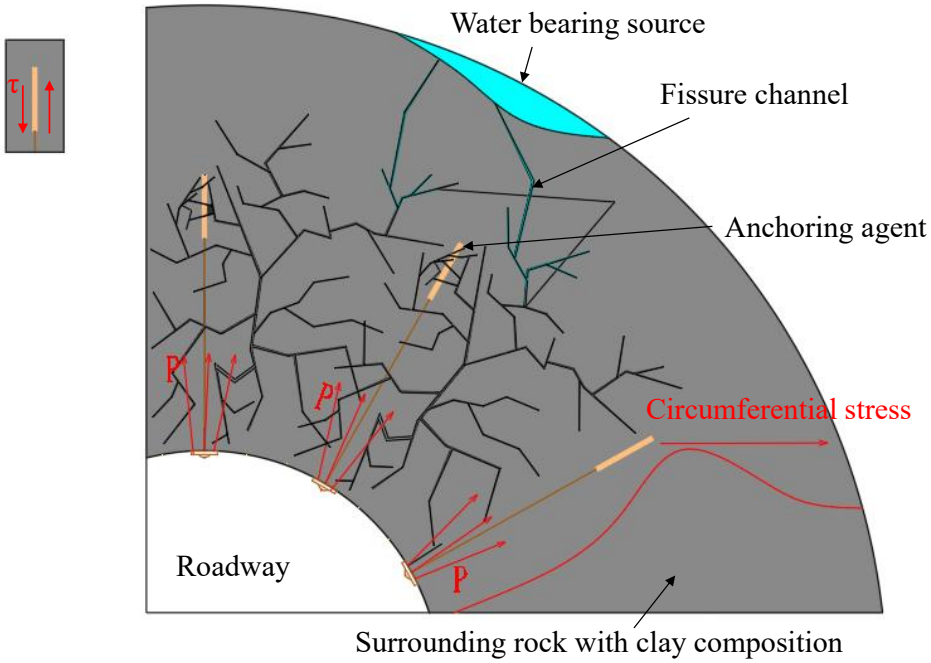


Fig.12 Schematic diagram of deformation and failure mechanism of roadway surrounding rock

5 Engineering application

5.1 Control principles

As analyzed above, four dominant factors induce deformation and failure of soft rock roadway surrounding rock under weak aquifer conditions, namely high-content water-sensitive clay minerals, weak anchoring foundation of bolts/cables, poor transmission effect of bolt/cable pre-stress, and low bearing capacity of surrounding rock, which are summarized as the "one water and three weaknesses" coupling characteristic. Beyond conventional support technologies, a "one isolation and three strengthening" control principle is proposed for soft rock roadways under weak aquifer conditions (**Fig.13**), detailed as follows:

(1) Isolation of water-rock contact: For newly excavated roadways, deep-hole grouting is implemented at the driving face before excavation to repel aquifers away from the roadway. Immediately after excavation, shotcrete is sprayed to seal exposed rock strata and maintain smooth excavation surfaces. For roadways requiring repair, quick-setting grouting materials with good fluidity are adopted for combined deep-shallow hole grouting to block water seepage channels and improve rock mass integrity. Meanwhile, water dripping on support components is drained via centralized pipelines. In short, "isolation" aims to prevent contact between seepage water and clay-bearing surrounding rock.

(2) Three strengthening measures after grouting: High-prestress full-length anchorage support is adopted. First, special waterproof expansion anchoring agents are used for one-time end anchorage to form firm bonding; then pre-tightening force equivalent to 30%–60% of the yield strength of anchor rods is applied; finally, full-hole grouting is conducted to realize full-length anchorage, and secondary high-strength material grouting is carried out on full-section surrounding rock to improve overall rock mass strength.

(3) Surface sealing after support completion: Additional shotcrete is applied to fully cover the tails of bolts/cables and all support components. The collaborative control principle of "one isolation and three strengthening" for soft rock roadway surrounding rock under weak aquifer conditions is illustrated in **Fig. 13**.

Water-rock isolation for soft rock roadways under weak aquifers: Surrounding rock with high clay mineral content contains abundant kaolinite, montmorillonite and illite, all belonging to lamellar aluminosilicate microcrystals. In water-bearing environments, water can enter and interact with clay minerals, with the degree of interlayer hydration and swelling varying with mineral type. Montmorillonite exhibits pronounced interlayer hydration and swelling, whereas kaolinite and illite generally show comparatively limited swelling. These water–mineral interactions can induce softening, dispersion, and disintegration of clay-rich rock, resulting in pronounced volume deformation and strength deterioration. Macroscopically, this phenomenon manifests in the 110207 transportation roadway as mudstone swelling, fragmentation, dispersive disintegration, or flocculent fluidization, accompanied by sharp strength loss. To avoid direct contact between water and soft rock, combined surrounding-rock grouting and surface shotcrete coating technologies are utilized to block groundwater infiltration and seal seepage channels, reducing water–rock interaction and maintaining surrounding-rock stability.

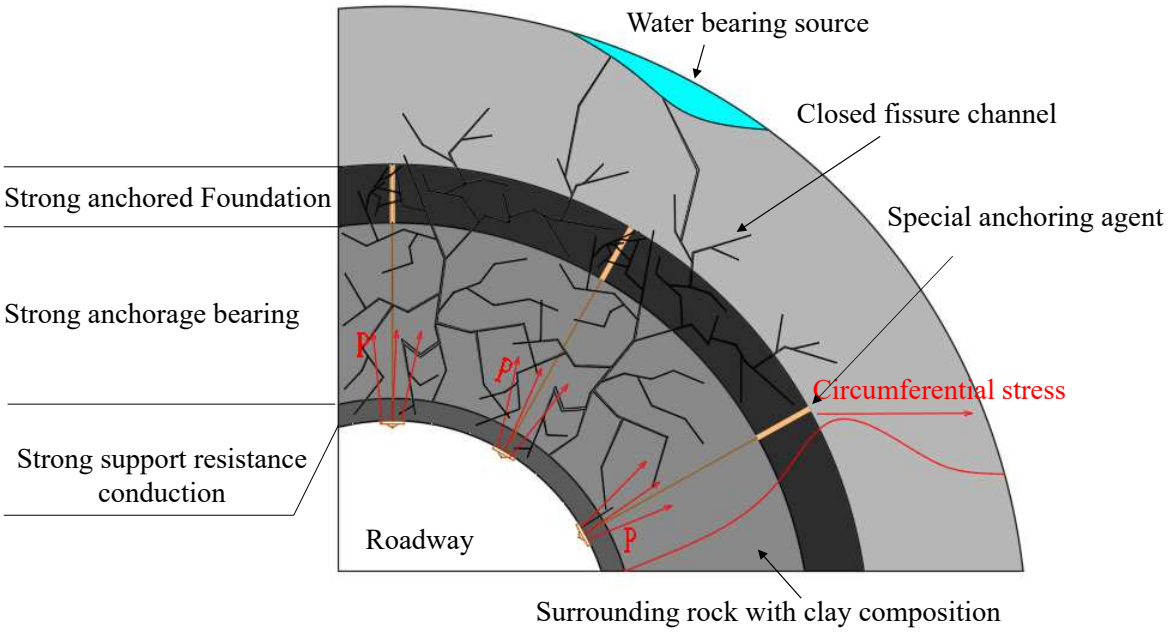


Fig.13 Control principle schematic diagram of "one isolation and three strengthening" for roadway surrounding rock

Strengthened anchorage foundation, stress transmission layer and bearing capacity for soft rock roadways under weak aquifers: After rock mass grouting, special anchoring agents and resistance-increasing anchoring section bolts/cables are adopted to reinforce the anchoring foundation. Large-area high-stiffness surface protection components and shotcrete layers on rock surfaces are used to strengthen the pre-stress transmission layer. High-strength anchor rods, secondary grouting, full-length anchorage and high pre-tightening force are integrated to reinforce the anchorage bearing layer. The collaborative grouting-anchoring support system with "three strengthening" measures can effectively restrain large deformation of surrounding rock. The total deformation of soft rock roadway surrounding rock under weak aquifers can be expressed by Eq. (1):

$$\sum \mu = \mu_e + \mu_p + \mu_w + \mu_q + \mu_b \tag{1}$$

Where μ_e, μ_p, μ_w, μ_q, μ_b represent elastic deformation, plastic deformation, water-induced swelling deformation, gravity-induced deformation and fragmentation dilatation deformation of surrounding rock, respectively. Elastic deformation μ_e is inevitable after roadway excavation; μ_w can be eliminated or reduced by isolating water from mudstone; μ_q is induced by natural self-stabilization of rock strata after excavation and exerts negligible influence on roadway stability.

Existing research demonstrates that μ_p and μ_b develop during plastic zone expansion of surrounding rock. Larger plastic zone radius R_0 corresponds to wider fractured zones and greater fragmentation dilatation deformation μ_b. Both deformations are closely correlated with the plastic zone radius R_0, which can be calculated via Eq. (2):

$$R_0 = a\left[\frac{(\sigma_v + c\cot\phi)(1-\sin\phi)}{p_i + c\cot\phi}\right]^{\frac{1-\sin\phi}{2\sin\phi}} \quad (2)$$

Eq. (2) indicates that the plastic zone radius R_0 is positively correlated with rock mechanical parameters c and φ, roadway radius a and insitu stress σ_v, while negatively correlated with support resistance P_i and support strength.

Grouting can increase the cohesion c and internal friction angle φ of the roadway surrounding rock. Applying sufficient pre-tightening force can enhance the support resistance P_i. Therefore, grouting combined with support can effectively restrain the expansion of the plastic zone radius R_0, thereby reducing μ_p and μ_b and bringing the large deformation of the roadway surrounding rock under control. Temporal and spatial relationship of the "one isolation and three strengthening" strategy for soft-rock roadways under a weak aquifer: The general principle is that isolating water from soft rock should precede the "three strengthening" support operations. Specifically, measures should be taken to divert water sources before roadway excavation. After excavation, grouting is applied to seal surrounding rock fractures or to cap or drain potential leakage points. Subsequently, the "three strengthening" operations—strengthening the foundation, surface, and bearing capacity are performed in sequence, ultimately realizing the collaborative control of "one isolation and three strengthening" for soft-rock roadways under a weak aquifer.

5.2 Optimized support design

Aiming at the characteristics of weak roof and sidewall rock mass with easily developed fractures in the 110803 working face transportation roadway, combined long and short cable bolt support is adopted. Short cable bolts provide timely active support to limit initial surrounding rock deformation, while long cable bolts realize coupled deep reinforcement to improve rock mass bearing capacity. Considering the argillaceous cemented floor prone to softening when exposed to water, short cable bolts are applied to primary floor support to enhance floor bearing capacity. Full-section shotcrete is adopted to resist weathering and water-induced argillization of roadway floor rock mass. The transportation roadway of the 110803 working face has an excavation width of 5500 mm and an excavation height of 3650 mm, excavated along the coal seam. The overall support layout is shown in **Fig. 14**. Eleven cable bolts are arranged on the roof, four cable bolts on each sidewall, and six cable bolts on the floor.

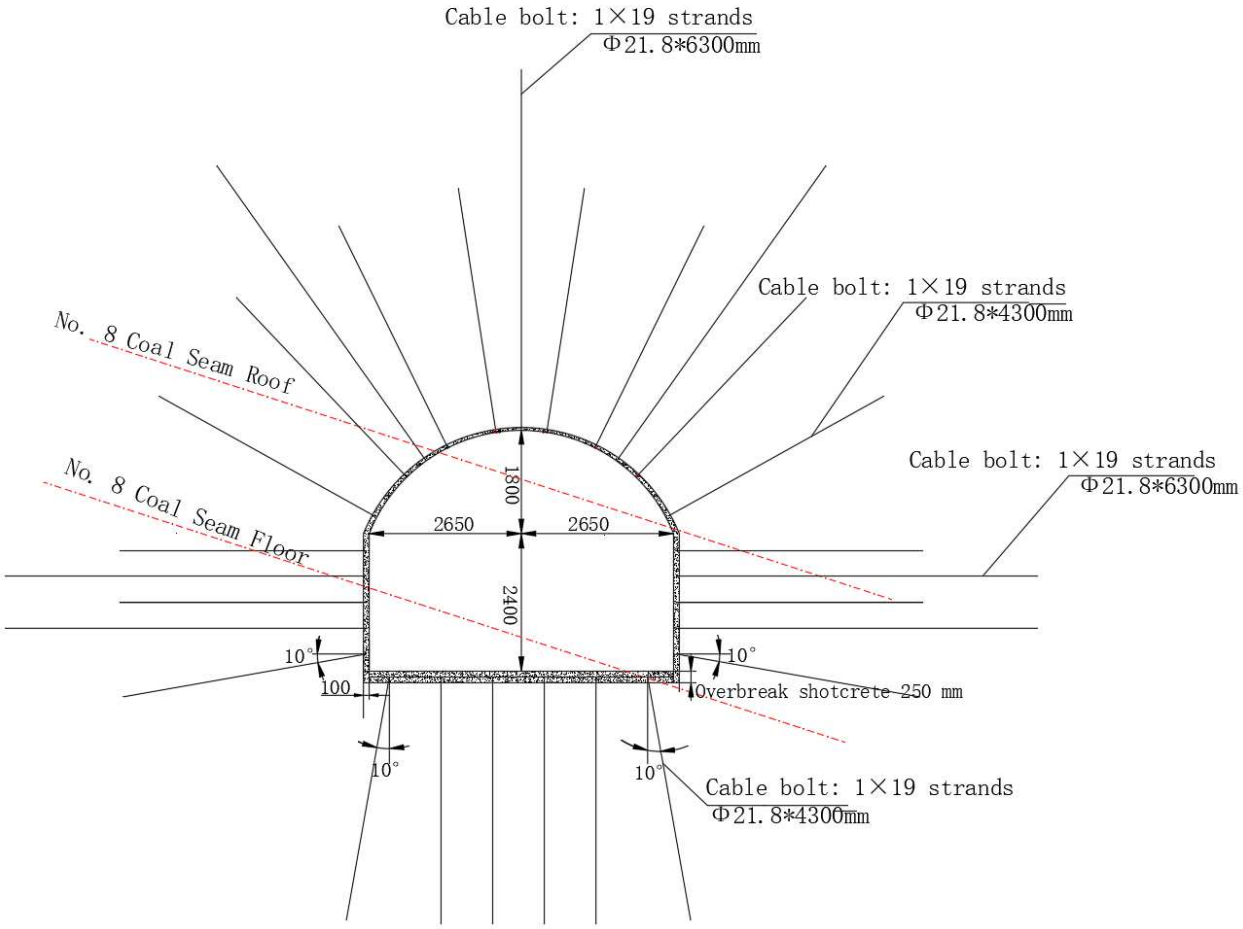


Fig.14 Overall support scheme for the transportation roadway of 110803 working face

Based on surrounding rock deformation characteristics and failure mechanisms, support parameters are optimized on the basis of the original scheme to address fractured surrounding rock, severe water seepage softening and coordinated deformation of roof, sidewalls and floor. An optimized support scheme centered on "collaborative support of long and short cable bolts with high pre-tightening force, combined control of shallow and deep bearing structures, integrated grouting reinforcement and shotcrete sealing" is proposed.

Combined support of 4300 mm short cables and 6300 mm long cables is adopted for the roof. Short 4300 mm cables construct a shallow bearing structure during primary support, and long 6300 mm cables anchor into deep stable rock strata in secondary support. The "1-2-1" layout improves roof integrity and deep bearing capacity. Sidewalls adopt the same graded long-short cable bolt support mode as the roof, with deep cables arranged in "2-2" layout to strengthen constraint and shear bearing capacity of sidewall rock mass and restrain sidewall bulging and spalling. Full-length grouted 4300 mm cable bolts are applied for floor support, integrating resin anchorage and grouting reinforcement technology to improve floor integrity and overall bearing capacity and effectively control floor heave.

High-strength steel strand cable bolts are used for all roadway sections with anchoring force no less than 280 kN and pre-tightening force no less than 250 kN. Reinforcement mesh and metal mesh are matched with shotcrete to form a surface sealing structure. The shotcrete thickness for roof and sidewalls is no less than 100 mm, and floor shotcrete thickness is no less than 250 mm. A multi-level collaborative support system of "shallow reinforcement – deep anchorage – surface sealing" is constructed to realize coordinated control of roof, sidewall and floor surrounding rock and guarantee long-term roadway stability.

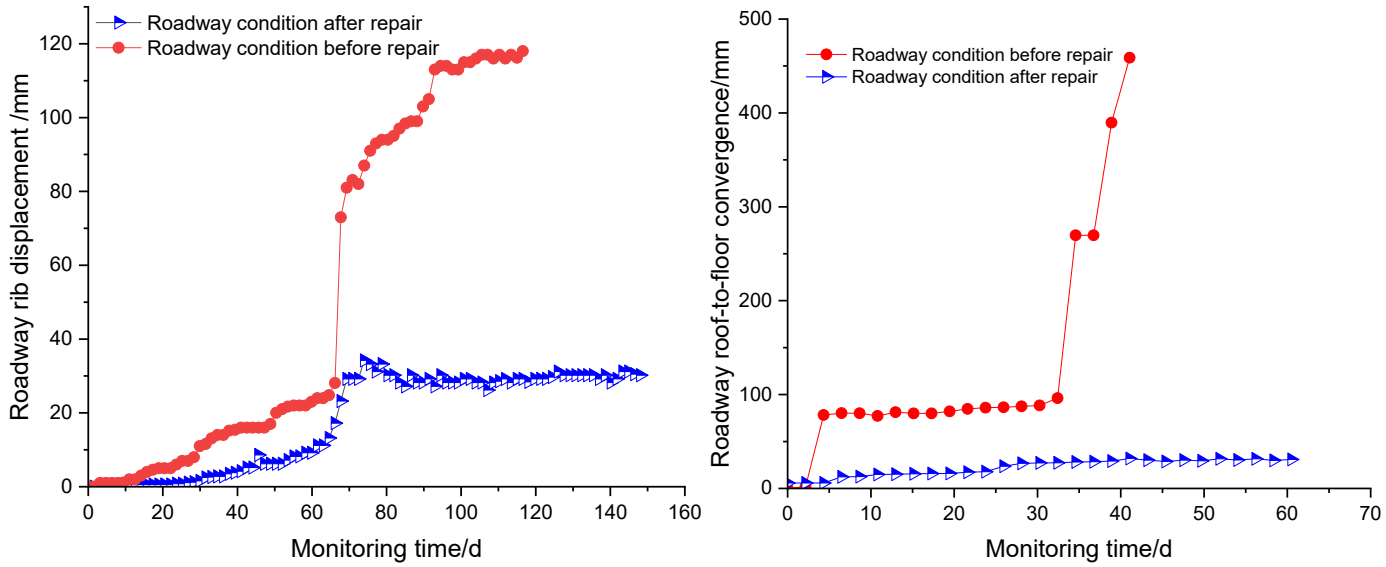
When water seepage occurs in roof cable boreholes, the seepage water will induce floor argillization and softening. Therefore, 6300 mm roof cable bolts are replaced with grouting cable bolts of identical length, or pre-grouting is implemented on roof rock strata to block water seepage channels. Grouting cable bolt specification: diameter 22 mm, structure

1 central hollow tube + 9 fine steel strands; grouting material consists of cement and additives, with typical grouting pressure of approximately 3 MPa.

5.3 Analysis of field application effect

(1) Monitoring results of station at 150 m

Field pressure monitoring data including surrounding rock displacement, roof separation, bolt and cable bolt stress are sorted and analyzed as follows. **Fig. 15** reveals a prominent stability difference of surrounding rock at the 50 m station of the 110803 transportation roadway before and after reinforcement. Severe surrounding rock deformation was observed before maintenance, while deformation was almost eliminated after the optimized support scheme was applied, maintaining long-term roadway stability. Before reinforcement, the roof-to-floor convergence reached 458.8 mm within 40 days of monitoring, and the rib-to-rib convergence continued to develop over more than 100 days and stabilized at approximately 115 mm, indicating severe and sustained deformation of the surrounding rock under the original support. After reinforcement, within an 80-day monitoring period, the roof-to-floor convergence was less than 50 mm and the rib-to-rib convergence was approximately 30 mm, with the surrounding rock deformation gradually converging in the later stage. Compared with the unreinforced conditions, the roof-to-floor convergence was reduced by approximately 89% and the rib-to-rib convergence by approximately 74%, demonstrating that the optimized support scheme effectively controlled the deformation of the water-rich soft rock roadway.



(a)Rib-to-rib convergence before and after reinforcement (b)Roof-to-floor convergence before and after reinforcement

Fig. 15 Surrounding rock displacement curves at the 50 m station of the 110803 transportation roadway

Fig. 16 shows the roof separation curve near the 50 m station of the 110803 transportation roadway.During monitoring, shallow roof separation displacement increased stepwise and finally stabilized at approximately 38 mm; deep roof displacement remained nearly zero without obvious variation. The roof separation value was consistently maintained at an extremely low level (< 2 mm) with minor fluctuation, and the curves flattened in the later monitoring period, indicating that surrounding rock deformation had basically converged. The support system effectively restrained roof separation and rock mass instability with favorable overall stability.

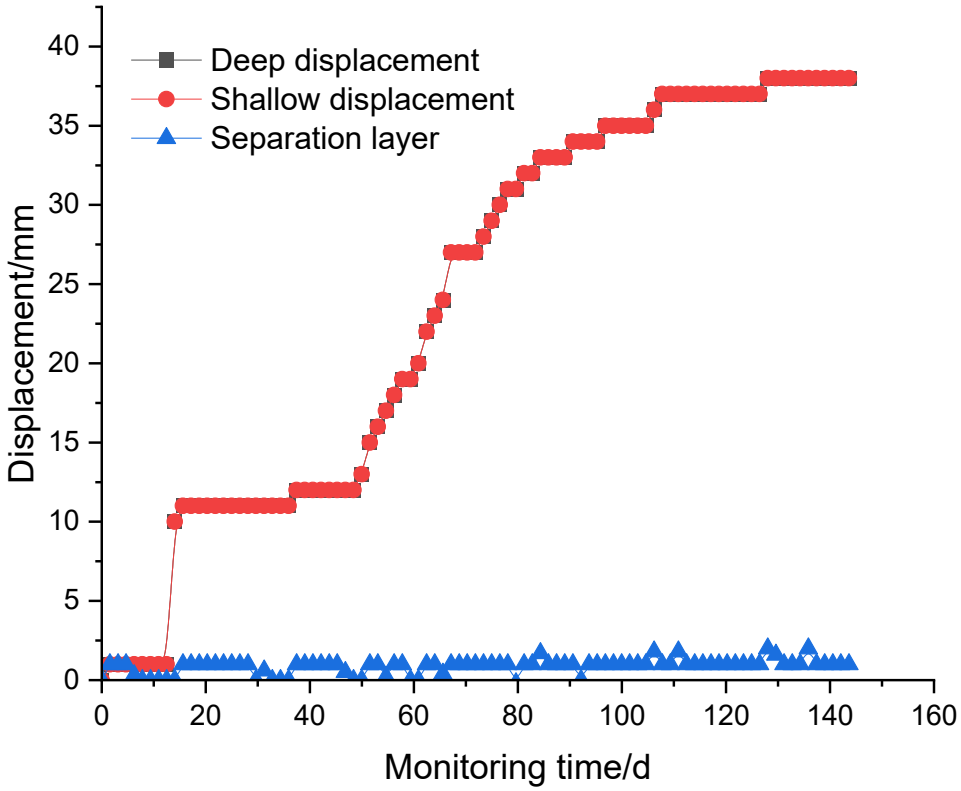


Fig. 16 Roof separation curve near the 50 m station of the 110803 transportation roadway

Fig. 17 presents the stress curve of rock bolts at the lower part of the working-face sidewall at the 50 m station. Rock bolt stress at the lower sidewall increased obviously from approximately 38 kN to 42 kN before reinforcement, and remained stable at about 42 kN after reinforcement without obvious fluctuation, proving progressive roadway stabilization after support renovation. Fig. 10-17 shows the stress curve of rock bolts at the lower working-face sidewall of the 50 m station: bolt stress rose from approximately 73 kN to 79 kN before reinforcement and stabilized at around 80 kN after renovation, indicating gradual roadway stability.

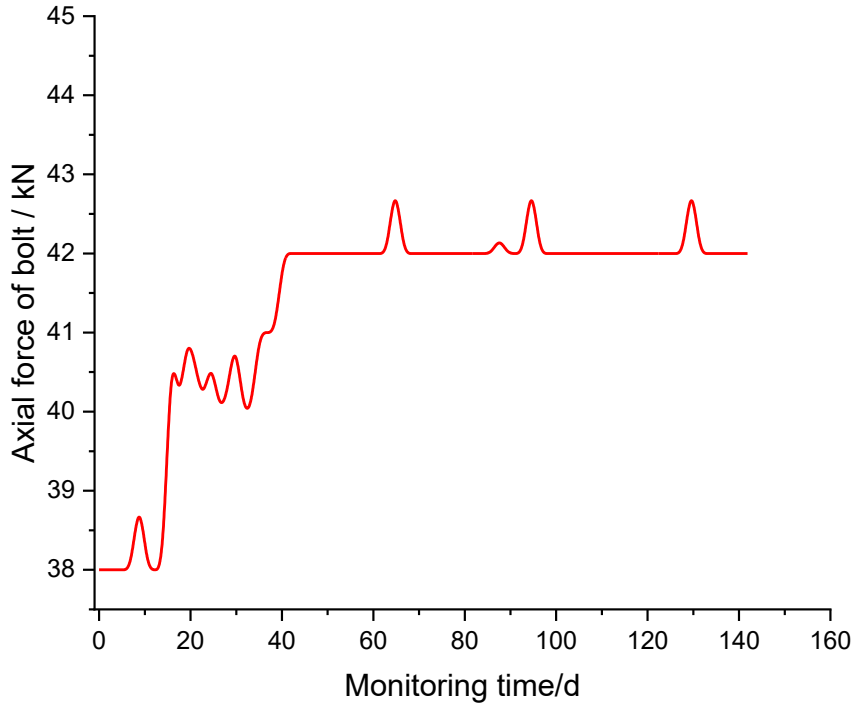


Fig. 17 Stress curve of rock bolts at the lower working-face sidewall of the 50 m station

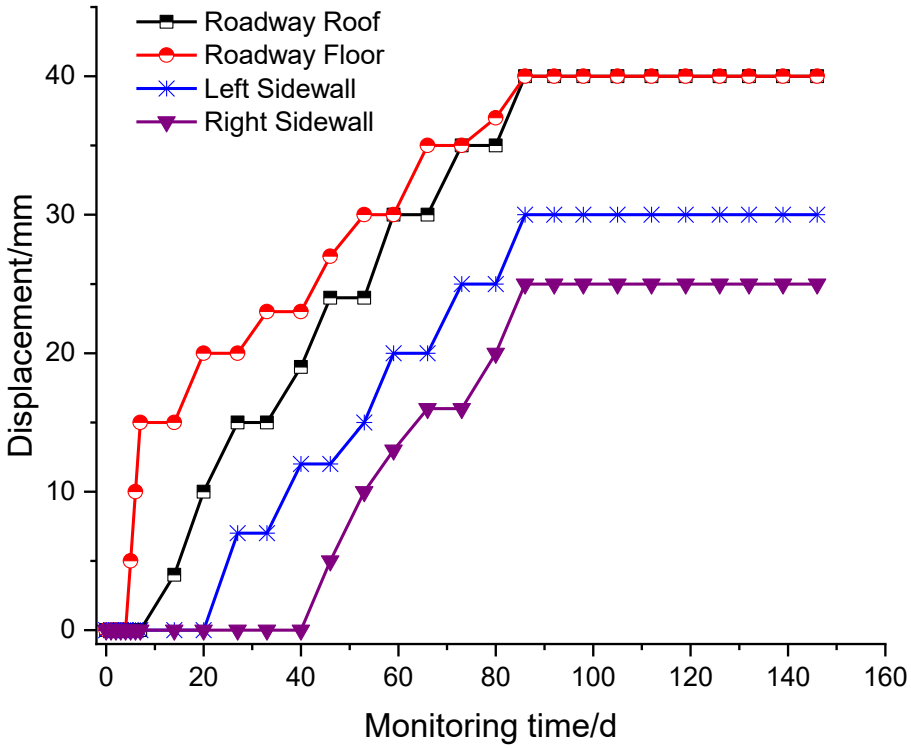
As shown in **Fig. 18**, synchronous displacement of shallow and deep monitoring points indicates no roof separation, and the measured data represent roof subsidence. Within 30 days before reinforcement, deep and shallow roof displacement jumped sharply to 18 mm; after renovation, the displacement increased slowly along an arc curve and stabilized at a total increment of 20 mm after 80 days.



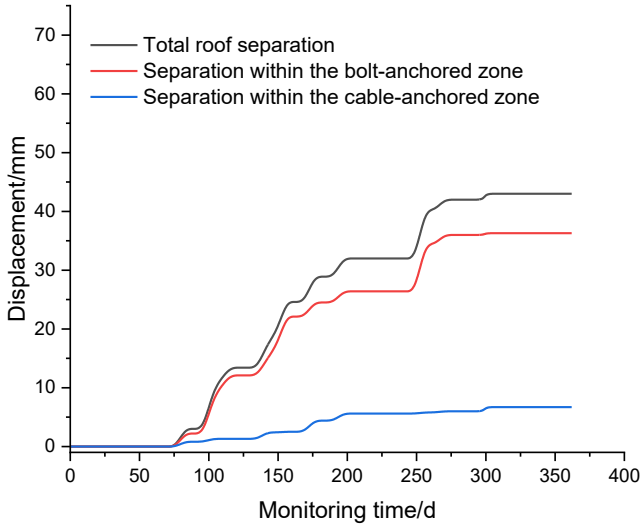
Fig. 18 On-site photo near the 50 m station of the 110803 transportation roadway

(2)Monitoring results of station at 1500 m

Fig. 19(a) demonstrates that roof separation follows the same variation law as roof-to-floor convergence: roof separation increased obviously within 0–100 days after roadway excavation and stabilized after 100 days, indicating gradual stabilization of surrounding rock in newly excavated roadways. **Fig. 19(b)** shows slight surrounding rock deformation within 100 days after excavation of the roadway at the 1550 m station of the 110803 transportation roadway, followed by long-term stable surrounding rock. The final roof-to-floor convergence was 85 mm and rib-to-rib convergence was 55 mm. Compared with the original support section with roof-to-floor convergence of 500 mm and rib-to-rib convergence of 400 mm, roof-to-floor convergence decreased by 83% and rib-to-rib convergence decreased by 86.25%, with a clear roadway section contour as shown in **Fig. 19(c)**.



(a)





(b) **(c)**

Fig. 19 Deformation characteristics of the surrounding rock in the 110803 transportation roadway (a) Surrounding rock displacement curve at the 1550 m station (b) Roof separation curve near the 1500 m station (c) Field photograph of surrounding rock damage near the 1500 m station

6 Conclusions

Field investigations indicate that the surrounding rock of the mining roadways in the 110803 working face consists predominantly of argillaceous weakly cemented soft rock affected by long-term water seepage. Continuous water–rock interaction progressively weakens the surrounding rock, whereas the existing low-prestress bolt–cable support system has limited capacity to restrain long-term deformation. Theoretical analysis, numerical simulations and field measurements show that the deformation evolution of the roadway surrounding rock comprises three stages: rapid growth, moderate growth and slow growth. Based on these findings, the main conclusions of this study are as follows:

(1) The progressive failure mechanism of interconnected weak zones in argillaceous weakly cemented soft rock is revealed. Roadway surrounding rock is characterized by coexistence of water-bearing high-clay strata, weak anchoring foundation, weak pre-stress transmission layer and low surrounding rock bearing capacity, summarized as the "one water and three weaknesses" coupling feature. Water-induced softening and swelling of roof rock mass is the primary inducement of severe roadway deformation and failure. Deformation and failure initiate at local weak zones and continuously expand to trigger overall surrounding rock instability, following the evolution law from local to global and from shallow to deep rock mass.

(2) A "one isolation and three strengthening" control mechanism targeting large-deformation argillaceous weakly cemented soft-rock roadways is proposed. The core concept is to iso-late water-rock contact via engineering technologies and to simultaneously strengthen the anchoring foundation, prestress transmission layer, and surrounding rock bearing capacity. On this basis, a full-enclosed pressure-bearing support theory of "roof control, sidewall reinforcement, and floor strengthening" is established.

(3) Several types of novel materials and equipment adapted to soft rock roadway support are developed: cable bolt resistance-increasing technology, optimizing anchorage section geometry to improve anchoring resistance; grouting locking devices; grouting sealing rubber plugs for bearing plates; waterproof expansion anchoring agents. A complete set of supporting technologies for argillaceous weakly cemented soft rock roadways is formed on this basis.

Author Contributions: G.G. (Gangye Guo): Data curation, Formal analysis, Investigation, Writing—Original draft; Yongzheng Wu and Genshui Wu: Project administration, Writing—Review and editing. All authors have read and agreed to the published version of the manuscript.

Funding: National Natural Science Foundation of China (52574115,52404121).

Acknowledgments: The authors would like to thank editors and anonymous reviewers for their time and effort in reviewing and improving this manuscript.

Data Availability Statement: The raw data supporting the conclusions of this article will be made available by the authors on request.

Conflicts of Interest: The authors declare no conflicts of interest.

References

[1] Yu, W., Li, K., Liu, Z., An, B., Wang, P. & Wu, H. Mechanical characteristics and deformation control of surrounding rock in weakly cemented siltstone. Environmental Earth Sciences 80, 337 (2021). https://doi.org/10.1007/s12665-021-09626-2

[2] Yu, W., Wu, G., Pan, B. et al. Laboratory and field investigations of different bolting configurations for coal mine roadways in weak coal strata. Bulletin of Engineering Geology and the Environment 80, 8995–9013 (2021). https://doi.org/10.1007/s10064-021-02477-y

[3] Wu, G., Yu, W., Pan, B. et al. Investigate on the mechanical properties and microscopic three-dimensional morphology of rock failure surfaces under different stress states. Geomechanics and Geophysics for Geo-Energy and Geo-Resources 10, 125 (2024). https://doi.org/10.1007/s40948-024-00833-2

[4] Wang, E., Yin, S., Chen, X., Gao, Z., Sun, A. & Yan, Y. Collaborative control technology and application of support and modification for soft-rock roadway in a kilometer-deep coal mine. Scientific Reports 15, 1979 (2025). https://doi.org/10.1038/s41598-025-86269-4

[5] Wu, G., Yu, W., Pan, B. et al. Failure mechanics mechanisms and permeability stage evolution models of limestone considering wave velocity and failure surface characteristics. Soils and Foundations 65, 101577 (2025). https://doi.org/10.1016/j.sandf.2025.101577

[6] Yu, W., Weng, H., Pan, B. & Liu, Z. Analysis of stress and deformation behavior of rock under equivalent non-uniform load conditions. Journal of Materials Research and Technology 38, 1419–1430 (2025). https://doi.org/10.1016/j.jmrt.2025.08.001

[7] Yu, W., Pan, B., Li, K. & Wu, G. Investigation on mechanical properties and dilatancy behavior of deeply buried mudstone: a comprehensive study. Construction and Building Materials 466, 140032 (2025). https://doi.org/10.1016/j.conbuildmat.2025.140032

[8] Jiang, Z., Guo, D., Xiao, C., Xie, S., Chen, D. & Lv, F. Failure mechanisms investigation for surrounding rock of soaking soft rock roadway in deep mine and preventative measures of cascade reinforcement control. Engineering Failure Analysis 182, 110147 (2025). https://doi.org/10.1016/j.engfailanal.2025.110147

[9] Zuo, Q., Li, X., Li, P., Deng, M. & Adoko, A. C. Surrounding rock instability mechanism for fault-crossing tunnels in water-rich soft rock. Bulletin of Engineering Geology and the Environment 83, 252 (2024). https://doi.org/10.1007/s10064-024-03753-3

[10] Wu, G., Yu, W., Zuo, J. et al. Experimental and theoretical investigation on mechanisms performance of the rock-coal-bolt (RCB) composite system. International Journal of Mining Science and Technology 30, 759–768 (2020). https://doi.org/10.1016/j.ijmst.2020.08.002

[11] Zhang, J., Wang, Y., Qi, X. & Zhu, T. Research on application of the bolt-truss coupling support technology in roadway with water-rich and soft rock. Frontiers in Earth Science 10, 842672 (2022). https://doi.org/10.3389/feart.2022.842672

[12] Wang, E., Yin, S., Cheng, Z., Xie, S., Chen, L., Kang, Q. & Duan, Y. Failure mechanism analysis of ultra-large-section soft-rock roadway in kilometer deep coal mine and its collaborative control of "grouting-anchoring-pouring". Engineering Failure Analysis 170, 109338 (2025). https://doi.org/10.1016/j.engfailanal.2025.109338

[13] Pei, H., Liu, X., Fan, D. et al. Large deformation mechanism and "stress relief-support reinforcement" synergetic control method of soft rock roadway in footwall of deep normal fault. Journal of Central South University 32, 3945–3967 (2025). https://doi.org/10.1007/s11771-025-5925-3

[14] Liu, S.-Q., Wang, H.-L., Lu, J. & Chi, M.-B. Deformation mechanism and support technology of deep asymmetrical soft rock roadway. Physics of Fluids 37, 037182 (2025). https://doi.org/10.1063/5.0263831

[15] Ma, Y., Wang, W., Fan, L., Yuan, C., Tian, X. & Shu, S. Research on crack distribution characteristics and control technology of surrounding rock in soft rock roadway under different lateral pressure coefficients. Energy Science & Engineering 12, 3852–3868 (2024). https://doi.org/10.1002/ese3.1841

[16] Sun, D., Zhang, C., Zhang, S., Xu, J., Tao, Z., Wu, M. et al. Hydraulic fracturing in-situ stress measurements and large deformation evaluation of 1000 m-deep soft rock roadway in Jinchuan No. 2 Mine, Northwestern China. Rock Mechanics and Rock Engineering 58, 2781–2801 (2025). https://doi.org/10.1007/s00603-024-04273-y

[17] Yan, L., Chang, J., Shi, W., Wang, T., Qiao, L., Guo, Y. & Wang, H. Creep deformation characteristics and control technology in deep mine soft rock roadway. Geomechanics and Geophysics for Geo-Energy and Geo-Resources 10, 144 (2024). https://doi.org/10.1007/s40948-024-00849-8

[18] Lin, W., Cheng, J., Li, D. & Dang, H. Deformation characteristics and control technology of roadway in water-rich soft rock. Geofluids 2022, 2234334 (2022). https://doi.org/10.1155/2022/2234334

[19] Lu, H., Yi, J., Liu, Q., Cao, A., Wei, A. & Zhang, K. A self-dissolved grouting reinforcement method for water-rich soft rock roadway. Bulletin of Engineering Geology and the Environment 81, 256 (2022). https://doi.org/10.1007/s10064-022-02744-6

[20] Zhang, W., Zhao, T. B. & Zhang, X. T. Stability analysis and deformation control method of swelling soft rock roadway adjacent to chambers. Geomechanics and Geophysics for Geo-Energy and Geo-Resources 9, 91 (2023). https://doi.org/10.1007/s40948-023-00635-y

[21] He, F., Zhai, W., Liu, W., Sun, N., Song, J., Zhang, J. & Wu, Y. Floor heave mechanism and control technique of water-rich soft-rock roadway in thick coal seam. Energy Science & Engineering 12, 5316–5327 (2024). https://doi.org/10.1002/ese3.1956

[22] Wang, F., Wu, C., Yao, Q., Li, X., Chen, S., Li, Y. et al. Instability mechanism and control method of surrounding rock of water-rich roadway roof. Minerals 12, 1587 (2022). https://doi.org/10.3390/min12121587

[23] Fan, H., Niu, X. & Li, S. Failure mechanism and control technology for coal roadway in water-rich area. Sustainability 15, 410 (2023). https://doi.org/10.3390/su15010410

[24] Li, L., Zhang, Y., Zhou, R., Qi, K., Zhang, Y. & Li, Q. Study on floor large deformation and failure mechanism of water-rich soft rock roadway. Scientific Reports 16, 14952 (2026). https://doi.org/10.1038/s41598-026-45877-4

[25] Yao, W., Wang, C., Pang, J., Liu, Y. & Zhang, J. Research and development of fully enclosed wire-shell support structure technology for deep soft rock roadway based on TRIZ theory. Scientific Reports 14, 3279 (2024). https://doi.org/10.1038/s41598-024-53972-7

[26] Yu, W., Wu, G., Pan, B., Wu, Q. & Liao, Z. Experimental investigation of the mechanical properties of sandstone-coal-bolt specimens with different angles under conventional triaxial compression. International Journal of Geomechanics 21, 04021067 (2021). https://doi.org/10.1061/(ASCE)GM.1943-5622.0002005

[27] Shan, R., Li, Y., Bai, H., Sun, P., Xiao, S., Wu, H. et al. Study on deformation and failure mechanism of semi-coal rock soft rock roadway and reinforcement support countermeasures of anchor cable with c-shaped tube. Engineering Failure

Analysis 178, 109708 (2025). https://doi.org/10.1016/j.engfailanal.2025.109708
[28] Xu, L., Wang, S., Elmo, D. & Ding, S. Mechanism and control of multi-level floor heave in soft rock roadway with straight-wall semicircular arch section. Tunnelling and Underground Space Technology 163, 106745 (2025). https://doi.org/10.1016/j.tust.2025.106745
[29] Guo, Z. & Gao, J. Compensation support technology and application of weakly cemented soft rock roadway. Bulletin of Engineering Geology and the Environment 84, 546 (2025). https://doi.org/10.1007/s10064-025-04532-4
[30] Liu, S., Yang, J., Cui, L., Zhang, Z., Fang, K. Microcrack evolution and mechanical performance of fiber-reinforced high water-resistant concrete backfill: A quantitative multi-scale study, Construction and Building Materials, 2026, 531: 146674. https://doi.org/10.1016/j.conbuildmat.2026.146674
[31] Li, Y., Ma, C., Zhang, L. & Li, B. Influence research for softening and swelling of weakly cemented soft rock on the stability of surrounding rock in roadway. Geofluids 2022, 6439277 (2022). https://doi.org/10.1155/2022/6439277